PERGAMON

International Journal of Heat and Mass Transfer 44 (2001) 3189–3199

International Journal of HEAT and MASS TRANSFER

www.elsevier.com/locate/ijhmt

Analysis of heat transfer enhancement in coiled-tube heat exchangers

Narasimha Acharya [a,*], Mihir Sen [a], Hsueh-Chia Chang [b]

[a] *Department of Aerospace and Mechanical Engineering, University of Notre Dame, Notre Dame, IN 46556, USA*
[b] *Department of Chemical Engineering, University of Notre Dame, Notre Dame, IN 46556, USA*

Received 28 September 1999; received in revised form 19 November 2000

Abstract

We analyze the phenomenon of steady heat transfer enhancement due to chaotic particle paths in steady, laminar flow through a tube. The performances of two different coils, one with regular mixing and the other with chaotic mixing, are numerically analyzed and compared. For the latter case, axially periodic boundary conditions over a unit cell are used. Velocity vectors and temperature fields are computed. Poincaré maps of fluid particles being repeatedly mapped from inlet to outlet of this cell are presented as function of system geometry. Point and periodic attractors with chaotic windows are found. Lyapunov exponents are used to establish the presence of chaotic mixing. Flow fields and isotherms are examined to reveal the mechanisms of enhanced heat and momentum transfer through modification of the wall and internal boundary layers. Spatially varying local and constant bulk Nusselt numbers and bulk friction factors are determined for a range of governing parameters.

1. Introduction

Heat transfer enhancement in internal flows without undue increase in pressure loss has been a goal in industry for a long time. Over the years, various means of increasing the rate of heat transfer have been proposed. Many of these active and passive methods enhance heat transfer by expelling temperature gradients through advective mixing. Of late, there has been a heightened interest in mixing studies [1,2]. A number of recent articles on fluid mixing have employed visual tools in the form of photographs and Poincaré sections for numerically computed flow fields [1,3]. The focus of this work is not on mixing itself but rather on the relationship between mixing and enhanced heat transfer. The term mixing used in this work is used to denote deformation or dispersion of material elements in a fluid. This view is consistent with the description suggesting that mixing can be viewed entirely in kinematic terms as the efficient stretching and folding of material lines and surfaces. In a flow field endowed with velocity and temperature gradients, mixing of material elements can lead to both momentum and thermal mixing. Thus, heat transfer enhancement may also be accompanied by undesirable pressure drop increases due to momentum transfer enhancement. However, it is shown in some recent studies that chaotic particle paths can be induced in laminar creeping flow. This suggests that, with a proper design of the mixing mechanism, heat transfer enhancement can be achieved with little increased pressure drop expenditure.

That mixing within recirculating zones in the flow can lead to significant increases in heat or mass transfer has been observed in many applications. In curved heat exchanger tubes, similar transverse recirculation is naturally present due to the centrifugal effects of tube curvature resulting in increased mixing and heat transfer compared to that obtainable in straight tubes. Numerous theoretical and experimental works have been directed at better understanding this phenomenon. These studies have focused on the potential of the secondary flows to increase heat transfer in coiled tubes as

* Corresponding author. Present address: Steag RTP Systems, Inc., 4425 Fortran Drive, San Jose, CA 95134, USA. Tel.: +1-408-935-2223; fax: +1-408-935-2700.

E-mail address: n.acharya@steag-rtp-us.com (N. Acharya).

0017-9310/01/$ - see front matter
PII: S0017-9310(01)00002-3

Nomenclature

a	tube radius
f	friction factor
G	pressure gradient parameter $= \rho\beta a^3/\mu^2$
$\mathbf{M}$	vector representing mean pressure gradient along coordinates
$Nu(\phi,z)$	local Nusselt number
$\overline{Nu}(z)$	peripherally averaged Nusselt number
$\overline{\overline{Nu}}$	peripherally and axially averaged Nusselt number
p	pressure
$\hat{p}$	periodic pressure deviation
Pe	Peclet number
Pr	fluid Prandtl number
$\mathbf{q}$	velocity vector
R	coil radius
r	radial coordinate
Re	Reynolds number $= 2\rho Wa/\mu$
T	fluid temperature
T_{bulk}	fluid bulk temperature
T_{w}	wall temperature
w	axial velocity component
W	average axial velocity
z	axial length
z_s	length after which coil switches axis

Greek symbols

β	negative of mean axial pressure gradient
γ	axial coordinate
γ_s	axial wavelength
δ	radius ratio a/R
ϕ	angular coordinate in plane normal to tube axis
θ	switching angle
μ	dynamic viscosity
ρ	fluid density
σ	source term in the energy equation

Other symbols

$*$	dimensional quantity
AA	alternating axis coil
CA	constant axis coil
ST	straight tube

compared to that in straight tubes. While recognizing the important role of secondary flows in enhancing radial transport, it is possible that a further enhancement may be obtained by suitably forcing the flow so as to render the particle trajectories chaotic. That trajectories that are chaotic can lead to better mixing has been observed experimentally and numerically [2–13].

In an earlier paper [4], we demonstrated that a time-periodic flow field whose particle paths are chaotic can also enhance heat dispersion and transport. This led to the construction of a coiled tube heat exchanger with an alternating coil axis where temporal forcing is replaced by a spatial one [14]. In steady flow within a tube, the axial coordinate is taken to be the analog of time and we have shown that by periodic changes in axis of a coiled tube, it is possible to produce chaotic pathlines in the flow. The periodic change is effected by perturbing the boundary to periodically alter the coil axis direction by a fixed angle resulting in the alternating-axis coil as in Fig. 1 (hereafter referred to as AA coil) as compared to a regular constant-axis helical coil (hereafter referred to as CA coil).

In earlier studies, the streamline or axial coordinate of a three-dimensional steady flow field is taken to be a time-like variable – the so-called Lagrangian particle perspective. This advection description is valid only if diffusion is negligible, or the Peclet number, Pe, is infinite. Whether the Lagrangian description remains valid at finite Pe will be scrutinized here. However, a more important distinction between a steady heat transfer

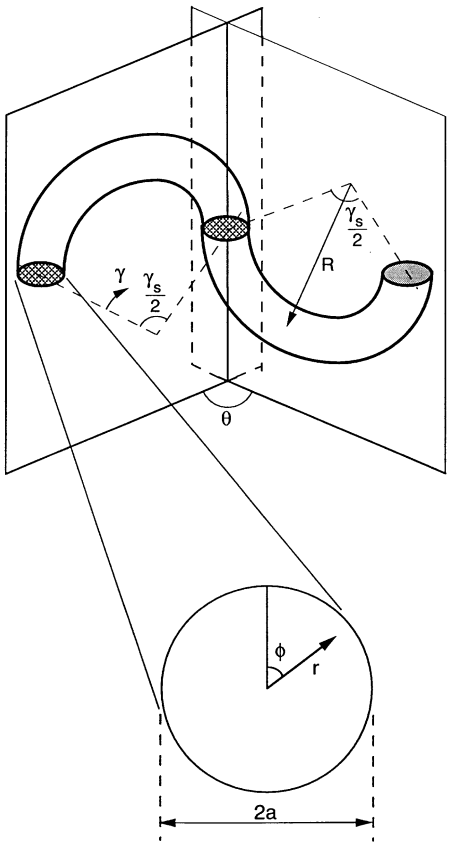

Fig. 1. Basic unit cell for alternating axis coil and coordinates.

problem and a time-periodic one is the existence of entrance thermal boundary layers. The enhanced temporal dispersion induced by time-periodic chaotic mixing often does not involve steady boundary layers. At most, transient boundary layers both within the flow and on the boundary appear periodically as convection balances chaotic dispersion. In contrast, steady heat transfer problems, like the heat exchanger coil, necessarily involve steady boundary layers. At large *Pe*, spatially periodic chaotic mixing can only serve to change the thickness of these boundary layers. Quantitatively, one hence expects a spatially-varying Nusselt number of a steady flow and a bulk Nusselt number for a time periodic flow. Spatial chaotic mixing is hence fundamentally different from temporal chaotic mixing.

The present work is aimed at clarifying some of the above-mentioned issues in mixing and its effect on heat transfer with a detailed numerical analysis of coiled tube heat exchangers for arbitrary curvature ratios. The study is carried out by comparing the thermal and hydraulic performance of the CA coil to that of the AA coil over different parameter ranges. We shall consider the case when the coil is periodically twisted in the downstream direction with a predefined switching angle, θ, i.e. the coil axis is rotated by θ. The twisting is performed about the axial coordinate with the first twist being θ and the second being $-\theta$ over a total axial length equal to half a coil loop. The switching action occurs after a distance $2\pi Rn$ coil lengths, where R is the radius of coiling. Thus $2n$ is the length of the unit cell. The axial length, z, and the axial switching length, z_s are defined relative to the mean coil radius as $z = R\gamma$ and $z_s = R\gamma_s$. The coordinate ζ is the non-dimensional distance along the cell, i.e., $\zeta = 2z/z_s$. Except where the switching length is being varied. n has been taken to be 1/4.

2. Governing equations

We use a toroidal coordinate system (r^*, ϕ, γ) where r^* and ϕ are the polar coordinates at a given axial position γ as shown in Fig. 1. The pitch of the coil is thus neglected. It is further assumed in the analysis that the flow is laminar, steady, with constant fluid properties, and with negligible viscous dissipation, gravity and buoyancy effects. In the following analysis, we extend the two-dimensional study of periodic heat transfer presented in Patankar et al. [15] to three-dimensional geometries, and apply it to the particular case of periodic flow and heat transfer in coiled tube heat exchangers.

For a straight tube and CA coil, the velocity and temperature fields exhibit a developing region with pronounced boundary layer structures near the inlet section and approach a fully developed value with distance downstream where the relevant axial gradients of the variables tend to zero. The thermally developed condition, on the other hand, is reached when the local Nusselt number approaches a constant value.

In contrast, the AA coil is axially periodic and features axially periodic velocity and thermal profiles. In this case, integrated measures over the unit cell approach a constant value in the fully developed limit. Periodic boundary conditions are assumed for the flows within this coil, so that the mathematical formulation becomes elliptic in all the three spatial coordinates. The fully developed state is defined by the periodicity conditions

$$\mathbf{q}^*(r^*, \phi, \gamma) = \mathbf{q}^*(r^*, \phi, \gamma + \gamma_s) = \mathbf{q}^*(r^*, \phi, \gamma + 2\gamma_s) = \cdots, \tag{1}$$

where $\mathbf{q}$ is the velocity vector, γ is the axial coordinate and γ_s is the axial angular wavelength. Following the analysis of Patankar et al. [15] and Lahbabi and Chang [16], the pressure is decomposed into that due to a constant overall axial pressure gradient β and a deviation from this $\hat{p}^*(r^*, \phi, \gamma)$, so that

$$p^*(r, \phi, \gamma) = -\beta\gamma + \hat{p}^*(r, \phi, \gamma). \tag{2}$$

The deviation is periodic so that

$$\hat{p}^*(r^*, \phi, \gamma) = \hat{p}^*(r^*, \phi, \gamma + \gamma_s) = \hat{p}^*(r^*, \phi, \gamma + 2\gamma_s) = \cdots. \tag{3}$$

For periodic geometries such as the AA coil, the local temperature field and Nusselt number will oscillate periodically even in the fully developed region. Appropriately scaled, the temperature field can be represented as

$$T(r^*, \phi, \gamma) = T(r^*, \phi, \gamma + \gamma_s) = T(r^*, \phi, \gamma + 2\gamma_s) = \cdots, \tag{4}$$

where the temperature has been non-dimensionalized as

$$T = \frac{T^* - T^*_{\mathrm{w}}}{T^*_{\mathrm{bulk}}(\gamma) - T^*_{\mathrm{w}}}. \tag{5}$$

The governing equations are non-dimensionalized using the radius of the tube, a, as characteristic length, $\beta a^2/\mu$ as a characteristic velocity, and $a\beta$ as a reference pressure difference. The continuity equation is then

$$\nabla \cdot \mathbf{q} = 0. \tag{6}$$

The momentum equation for a Newtonian fluid is

$$G\left(\frac{1}{2}\nabla(\mathbf{q}\cdot\mathbf{q}) - \mathbf{q}\times\nabla\times\mathbf{q}\right) = -\nabla\hat{p} + \mathbf{M} + \nabla^2\mathbf{q}, \tag{7}$$

where

$$\mathbf{M} = \left(0, 0, \frac{1}{1 + \frac{1}{2}r\delta(\sin\phi + \sin(\phi+\theta))}\right)^{\mathrm{T}}, \tag{8}$$

$r = r^*/a$ is the non-dimensional radial coordinate, $\delta = a/R$ is the radius ratio, $G = \rho\beta a^3/\mu^2$ is a pressure

gradient parameter and is related to the flow Reynolds number $Re = 2\rho W^* a/\mu$ by

$$Re = 2GW. \tag{9}$$

The first term on the right-hand side of Eq. (7) corresponds to the deviation pressure while **M** is a momentum source term due to the overall axial pressure gradient.

The energy equation can be written as

$$\nabla \cdot (\mathbf{q}T) = \frac{1}{GPr}\nabla^2 T + \sigma. \tag{10}$$

The source term

$$\sigma = \frac{1}{\hat{T}}\left\{\frac{2}{GPr}\nabla T \cdot \nabla \hat{T} + \frac{T}{GPr}\nabla^2 \hat{T} - \mathbf{q}T \cdot \nabla \hat{T}\right\}, \tag{11}$$

where

$$\hat{T} = T^*_{\text{bulk}} - T^*_{\text{w}}, \tag{12}$$

σ appears in Eq. (10) due to the form of the non-dimensionalization since T^*_{bulk} depends on the axial coordinate γ. For each problem there is a specific value of σ satisfying the equation and boundary conditions.

The appropriate hydrodynamic and thermal boundary conditions at the wall are that at $r = 1$, $\mathbf{q} = 0$ and $T = 0$. In addition we have the periodicity conditions defined by Eqs. (1), (3) and (4).

The local Nusselt number at a point on the wall is given by

$$Nu(\phi, \gamma) = 2\frac{\partial T}{\partial r}. \tag{13}$$

This can be integrated over ϕ to give the peripherally averaged Nusselt number $\overline{Nu}(\gamma)$ at a given z section. For the AA coil this can be further integrated over a unit cell to give $\overline{\overline{Nu}}$.

3. Numerical scheme

The Eqs. (6), (7) and (10) are reduced to a set of algebraic equations using the control volume method. The domain is discretized in the toroidal coordinate system based on uniform increments in the radial, angular and axial coordinates. A staggered grid is employed such that the elemental control volumes for the radial, angular and axial velocities are staggered in the positive direction along each coordinate by half a control volume each. The nodes at which the variables are computed are placed centrally within each elemental control volume. Further details can be found in [17].

Discretized versions of the governing equations are obtained by applying conservation of mass, momentum and energy to each elemental control volume. Mass fluxes at the faces of the elemental control volume are obtained by linear interpolation between the nodal values. Momentum fluxes at the boundaries are obtained by a hybrid scheme. The pressure correction equation is obtained from the continuity equation by using the pressure-velocity coupling as in the SIMPLE algorithm with the approximation suggested by Van Doormaal and Raithby [18]. The pressure field is continually updated in the calculation procedure by defining an arbitrary pressure level, equal to the pressure at one of the interior grid points.

For each set of parameters G, δ and θ, the flow field is determined. Integration of the axial velocity $w(r, \phi, \gamma)$ over any cross-section then gives the average flow velocity W which is independent of z. From this Re can be determined using equation (9). The numerical results are validated against known theoretical and experimental results available in the literature. The flow field is validated against Dean's solution [19] in the low Dean number limit and the friction factor as well as the Nusselt numbers were compared over a range of Reynolds numbers. A typical mesh used for the computations was $(40 \times 48 \times 40)$ in the (r, ϕ, γ) coordinates.

4. Chaotic particle paths and the enhancement mechanism

In straight tube flows, repeating developing flow patterns can be generated by means of physical obstructions located periodically in the path of the flow. This serves to destroy the limiting parallel flow reached in the developed state and contributes a radial flow component which leads to increased momentum and thermal mixing. In coiled tubes, since the fully developed flow regime already features a transverse flow, repeated developing flow patterns are easily generated by the essentially passive arrangement of modifying the direction of the centrifugal force by rotating the coil axis with no additional flow obstructions.

For the CA coil, in the fully developed flow condition the gradient $\partial w/\partial z$ is identically zero. The cross-sectional flow field satisfies the continuity equation at all points and is thus Hamiltonian. For the AA coil however, since $\partial w/\partial z \neq 0$ even in the fully developed limit, the transverse flow can be locally dissipative, i.e. non-area preserving, at every point on a cross-section even though it is globally conservative over the entire cross-section, the integral of $\nabla_T \cdot \mathbf{q}_T = -\partial w/\partial z$ being zero over any cross-sectional area. In the stroboscopic maps of the cross-sectional flow field of the AA coil, fixed points may sometimes represent axially periodic particle trajectories rather than attractors.

Figs. 2(a)–(d) show the Poincaré maps for a range of switching angles from 0° to 90° obtained for a fluid element traversing 4500 unit cells in the axial coordinate. Since the G has been kept constant at 400, the values of Re vary in the range of 81–83, approximately. There are

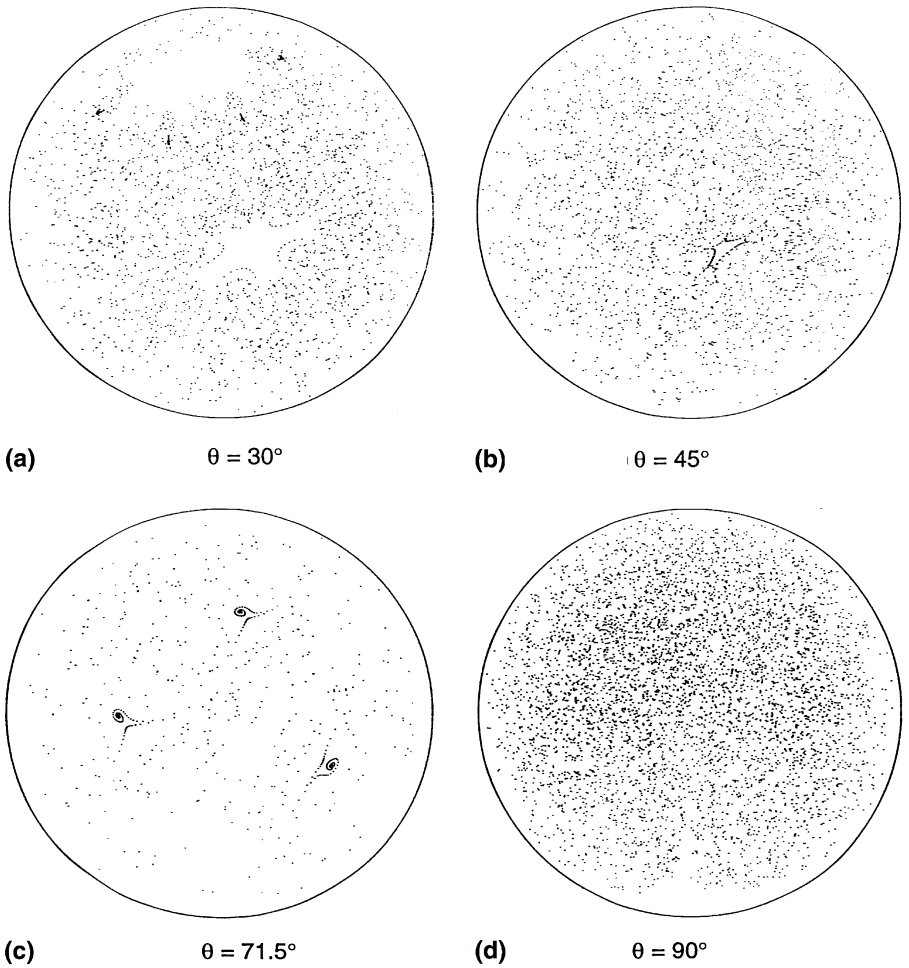

Fig. 2. Poincaré sections for flow field of AA coil for different switching angles, $G = 400, \delta = 0.2, z_s = \pi/2\delta$.

two elliptic fixed points for the case of $\theta = 0$, which represents a CA coil. As shown in Table 1, except for switching angles in the region of $\theta = 45°$ and $\theta > 72°$, single or multiple periodic points are observed in the map. For $\theta = 15°$, the fixed points are truly periodic. This means that the particle trajectories passing through the fixed points displayed are periodic with axial periodicity of n unit cells when there are n fixed points in the map. The parameters for this table are the same as those in Fig. 2. For $\theta = 45°$ and for $\theta > 72°$, an infinite number of fixed points are observed in the Poincaré map. All fixed points are unstable in this limit and the radial position of a neutrally buoyant particle undergoes chaotic variation downstream under the Poincaré map for all values of δ and Re [14]. It is only at these switching angles that the particle path is truly chaotic and a positive Lyapunov exponent can be calculated. Chaotic mixing is lost at other switching angles because of the coupling between the transverse flow and the axial flow at sufficiently large δ which renders the transverse flow dissipative. There is hence a qualitative difference in the transition sequence to chaos in a flow with a conservative transverse flow, like the Dean's flow at small δ, where the mechanism is a Melnikov bifurcation and the dissipative transverse flow here where chaotic regions are interspersed with regions of periodicity. The Lyapunov exponent calculated using the method of phase space reconstruction [20], yields a value of 1.14 for $G = 400, \delta = 0.2$ and $\theta = 90°$. In constrast, the value for the CA coil asymptotes to zero within three significant digits. Thus, the trajectories of the AA coil at $\theta = 90°$ are chaotic while those of the CA coil are not. We have previously shown [14] that the Lyapunov exponent for the AA coil, calculated using the simplified flow field given by Dean's equations and an assumption of zero development length, shows a value of 1.5 for the same switching angle. Hence the dissipation mechanism that arises at finite δ serves to reduce the degree of mixing,

Table 1
Location and unit-cell periodicity of attracting fixed points (r, ϕ) for different switching angles θ ($G = 400, \delta = 0.2, z_s = \pi/2\delta$)

$\theta(^\circ)$	r	$\phi(^\circ)$	Periodicity
0	No attracting fixed points		
15	0.64	6	Period 1
	0.35	157	Period 1
25	0.69	353	Period 1
28	0.69	354	Period 1
30	0.76	310	Period 4
	0.80	21	Period 4
	0.46	12	Period 4
	0.43	323	Period 4
31	0.23	148	Period 1
35	0.24	135	Period 1
40	0.26	133	Period 1
43	0.20	135	Period 1
45	No attracting fixed points		
46	0.25	139	Period 1
50	0.21	137	Period 1
60	0.76	333	Period 1
65	0.85	325	Period 2
	0.62	327	Period 2
70	0.47	320	Period 2
	0.89	314	Period 2
70.5	0.48	320	Period 2
	0.89	313	Period 2
71	0.51	272	Period 3
	0.64	113	Period 3
	0.52	6	Period 3
71.5	0.47	267	Period 3
	0.59	114	Period 3
	0.50	10	Period 3
$\geqslant 72$	No attracting fixed points		

assuming that the Lyapunov exponent is a measure of mixing. Of course, while the Dean's flow is chaotic for all switching angles, the real flow is chaotic only for some switching angles. Since our interest here is motivated by the application of this mechanism for a heat transfer process, we shall restrict ourselves to the observation that, though dispersion is enhanced for the AA coil by chaotic mixing as evidenced by a positive Lyapunov exponent, this does not in itself ensure improved heat transfer performance for such a coil.

In order to understand the mechanism responsible for the heat transfer enhancement in the alternating axis coil, we begin by looking at the transverse flow field. Figs. 3(a)–(d) show the cross-sectional velocities at various axial distances along the unit cell as indicated. It is noticed from the figure that within a short distance after the plane of coil switch, the vortex pair is rotated by an angle approximately equal to the switching angle. Following this, the local details of the flow evolve over a much longer length.

The transverse flow field for the CA coil shows the existence of a separatrix streamline, connecting the two hyperbolic stagnation points, between the counter-rotating vortex pair along which flow is advected by the secondary vortices. For $Pe \gg 1$, a thermal boundary layer of thickness $Pe^{-1/2}$ also forms across the separatrix where diffusive heat transfer in the normal direction is balanced by tangential convective flux. Fig. 4 shows the isotherms in the thermal developing region for the CA coil at $Pe = 1000$. Within each vortex, there exists a hot spot with uniform temperature due to convective mixing accompanied by large normal gradients at the inner region of the boundary layer. By invoking the alternating axis mechanism, the thermal boundary layer across the separatrix is destroyed leading to convective exchange of energy across this barrier. Consequently, a major mechanism by which chaotic mixing of an AA coil enhances heat transfer is by eliminating the internal boundary layer at the separatrix to homogenize the interior temperature.

But the above mechanism is only effective at high Pr. In our earlier study of a low Pr CA coil [14,21], it was found that diffusion dominates in the entire tube and, instead of an interior thermal boundary layer at the separatrix, a hot spot is formed at the tube center at an axial distance at which the Nusselt number curve exhibits a minimum. The subsequent increase in the transverse averaged Nusselt number in the thermally developing region for low Pr fluids as shown in Fig. 5 is due to the downstream eccentric displacement of this hot spot under the combined action of the axial and secondary flow. This coupling between the flow and temperature fields leads to the continued presence of a thin thermal boundary layer over a portion of the tube cross-section near the stagnation point region even in the fully developed condition, resulting in an efficient heat transfer process. Since there is no internal thermal boundary layer in this case, and since the convective flux is small compared to the diffusive flux, rotation of the coil axis merely displaces the hot spot across the tube cross-section without significantly altering the temperature profile. We see here that for the chaotic mixing to result in a manifestly larger heat transfer, convective heat transport has to be significantly larger than diffusive heat transport. As seen from Fig. 6, for low Pr fluids, the Nusselt number for the CA coil may actually be higher than that of the AA coil. It may also be observed that the Pr effect at a given switching angle is independent of the flow Lyapunov exponent. This is so since the Lyapunov exponent is completely determined from a specification of the curvature ratio, δ, and the pressure gradient parameter, G, and is then unaffected by the choice of the Prandtl number. In particular, in Fig. 6, though the pathlines are chaotic for the AA coil for each of the three cases shown, the Nusselt number ratio relative to the CA coil is greater than one only for

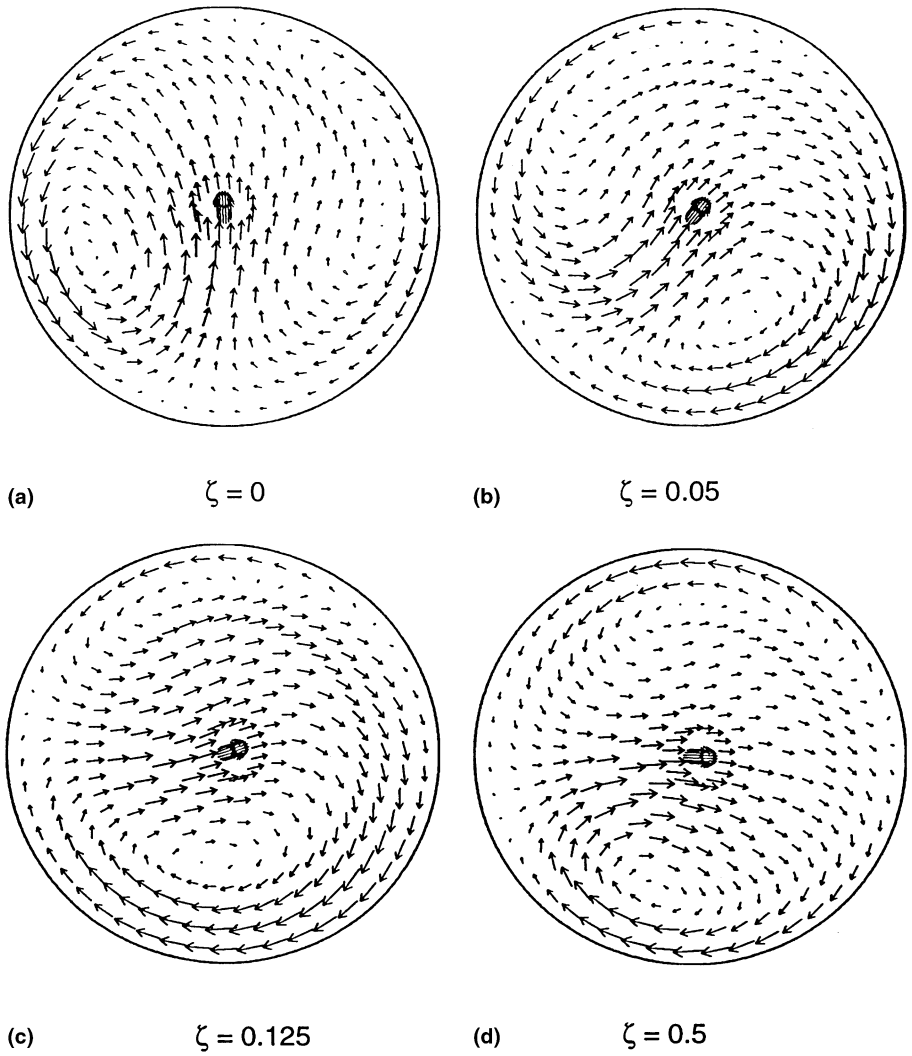

Fig. 3. Cross-sectional velocity vector field along the unit cell for AA coil; $G = 5500$ ($Re = 685$), $\delta = 0.1$, $\theta = 90°$, $z_s = \pi/2\delta$.

large Pe. Thus the chaotic mixing effect, while being intimately related to heat transfer enhancement as it specifies the optimal switching angle, does not provide full details of the mechanism involved.

The development of the internal boundary layer at large Pr also determines the optimal switching length of the AA coil. In essence, the periodic switching eliminates this interior thermal boundary layer. There are hence two important mechanisms in the heat transfer enhancement. One is the minimization of the interval over which an interior boundary layer exists and the other is the maximization of mixing across this boundary layer once it is broken. The second mechanism can be enhanced by chaotic mixing while the first is accomplished by selecting the optimal switching length. We shall study these observations with the following numerical studies.

5. Heat transfer and pressure drop results

The transverse averaged Nusselt number of an AA coil, plotted in Fig. 7 for $G = 5500$ which corresponds to $Re = 685.3$ for the CA coil, and $Re = 684.8$ for the AA coil, shows a continuous variation along the unit cell. Contrast this to the case of the constant axis coil, in which the Nusselt number goes to a constant for these parameters, and it becomes clear that the elliptic influence of the conditions occurring due to axis switching permeates throughout the length of the unit cell. In this particular figure, the non-dimensional axial length, which represents the absicca ζ, has been normalized by the length of the unit cell, γ_s/δ, i.e., $\zeta = z/2z_s$. A point of interest here is that even though the flow field repeats in axial lengths of γ_s/δ, the peripheral averaged Nusselt

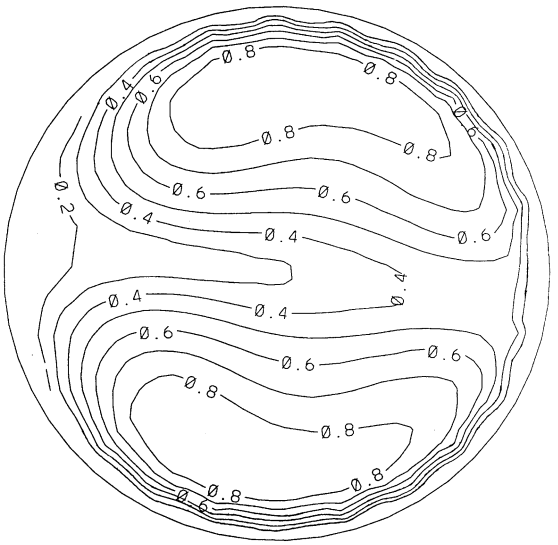

Fig. 4. Isotherms for CA coil at $z = 80$. $G = 5500$ ($Re = 685$), $\delta = 0.1$, $Pr = 1$.

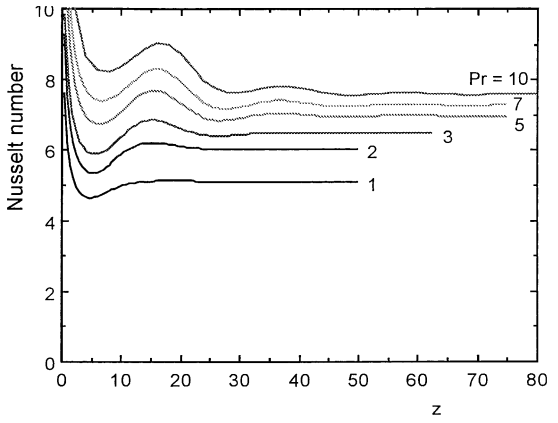

Fig. 5. Peripherally averaged Nusselt numbers at entrance to CA coil; $G = 400$ ($Re = 81.3$), $\delta = 0.2$.

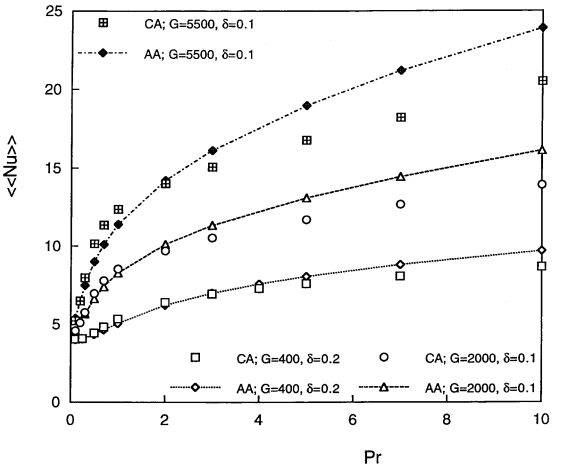

Fig. 6. Nusselt number dependence on Prandtl number for CA and AA coils.

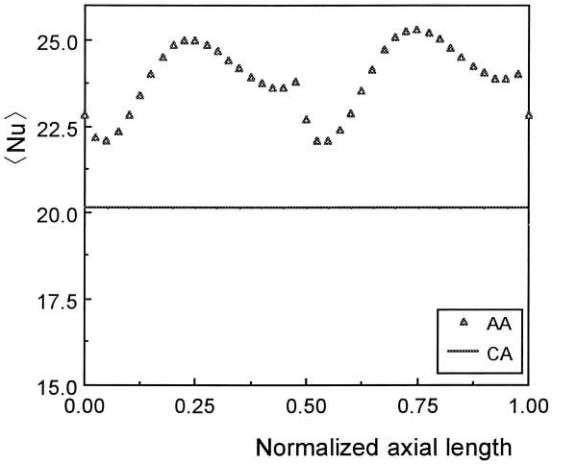

Fig. 7. Peripherally averaged Nusselt number; $G = 5500$ ($Re = 685$), $\delta = 0.1$, $Pr = 10$. For AA coil, $\theta = 90°$.

number as shown in Fig. 7 repeats periodically in axial lengths of $\gamma_s/2\delta$.

In order to frame the discussion in standard terms and to facilitate comparison to straight tube data, the pressure drop data is expressed in terms of the friction factor. For any internal flow the friction factor, f, can be written in terms of the pressure drop parameter, G, and the Reynolds number, Re, as

$$f = 16\frac{G}{Re^2}. \tag{14}$$

The friction factor is thus a mean value over the unit cell of interest. For laminar flow in a straight tube, the pressure drop is proportional to the flow rate, $G = 4Re$. For curved tubes in general, the $Re = Re(G, \delta, \theta)$ function is not known, but can be easily determined numerically from Eq. (9) once the steady state flow field is established.

Figs. 8(a) and (b) contrast the friction factor ratio and the Nusselt number respectively for the two coils. Though the f value for coiled tubes are much higher than that for straight tubes due to the recirculating transverse flow, the friction factor ratio is seen to be approximately the same for the two coils with the difference being of the order of 1%. As discussed earlier, the Nusselt number is a function of the Prandtl number and is about 10% more for the alternating axis coil at a Prandtl number of 10. For this set of data, the coil axis was switched by 90° after each half of a unit cell.

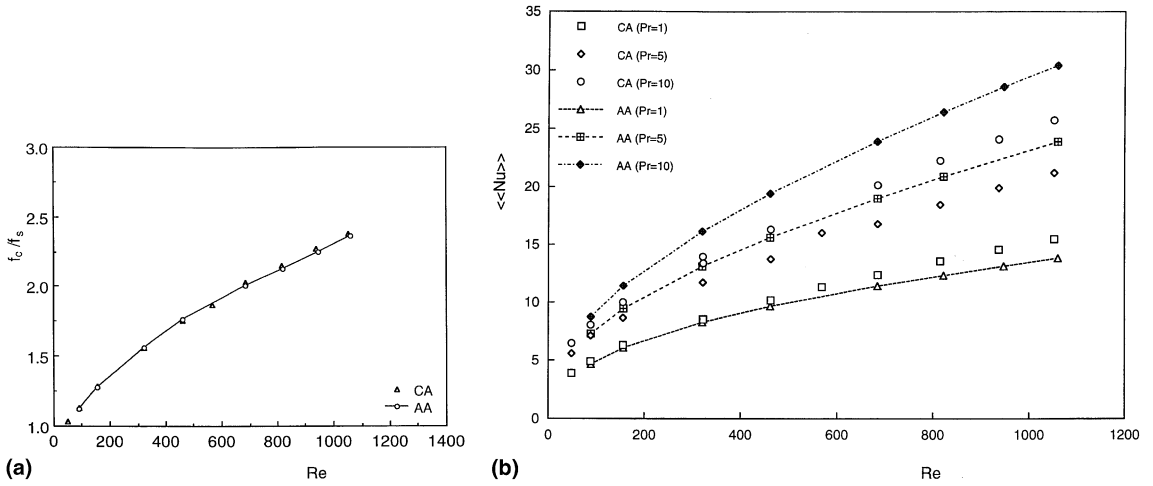

Fig. 8. (a) Variation of friction factor ratio with Reynolds number, $\delta = 0.1$. For AA coil, $\theta = 90°$. (b) Variation of Nusselt number with Reynolds number, $\delta = 0.1$. For AA coil, $\theta = 90°$.

Despite the considerable mixing achieved in case of the AA coil as evidenced by the Poincare maps of Fig. 2, the overall pressure drop for the AA coil is not much different from that of the CA coil as seen from Fig. 8(a). This is so because to leading order, the pressure drop is a function of the mean axial flow velocity, which is larger than the cross-sectional velocities by almost an order of magnitude over the entire range of Reynolds numbers examined here. Consequently, the change in cross-sectional velocity field between the CA and AA coils only marginally influences the mean flow field. The Nusselt number, on the other hand, relates to wall heat transfer and is affected to leading order by the transverse flow. For large Pr, the AA mechanism is therefore a viable means of obtaining significant heat transfer enhancement with little extra expenditure in pressure drop.

Fig. 9 shows the friction factor and Nusselt number ratios as a function of switching angle. The Reynolds number varies between a minimum of 69.3 for $\theta = 135°$ to a maximum of 74.1 at $\theta = 0$. The Prandtl number used for the Nusselt number calculations is ten. Similar variation of the Nusselt number and the friction factor is also observed for $G = 3250$ ($Re = 300$). This case is omitted for reasons of space. The maximum enhancement is attained roughly at $\theta = 120°$, as is consistent with our Poincaré map analysis. It should also be noted that not all switching angles result in an increase in the Nusselt number. For example, at $\theta = 180°$, the Nusselt number for the alternating axis coil is actually lower than the constant axis coil by about 20%. The pressure drop shows a variation of $\pm 4\%$ in the range of switching angle θ examined here.

The minimum in the Nusselt number curve seen in Fig. 9 is related to the interaction of the developing flow field with the cross-sectional temperature field. At a switching angle of $\theta = 180°$, the hot spot at the tube center gets

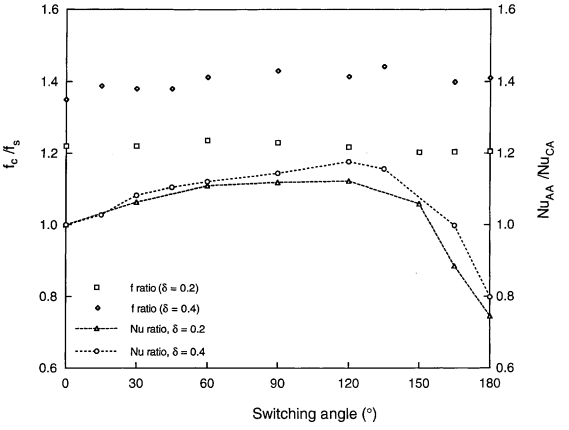

Fig. 9. Friction factor and Nusselt number ratios as a function of switching angle, $G = 400$.

displaced eccentrically across the tube cross-section as one progresses along the axial coordinate, but its transverse motion is reversed before it reaches the wall. This leads to reduced mixing near the boundary and inefficient heat transfer. The periodicity of this modulation depends on the switching length. In this particular example, the switching length is chosen to be less than the thermal development length. It is thus noted that the switching length is an important parameter controlling the Nusselt number. For $Pr < 10$, the Nusselt number is weakly sensitive to the switching length, provided the switching length is kept equal to or larger than 1/4th of a coil loop.

6. Nusselt number correlations

On the basis of the numerical data, the Nusselt number is correlated against δ, Re and Pr in terms of

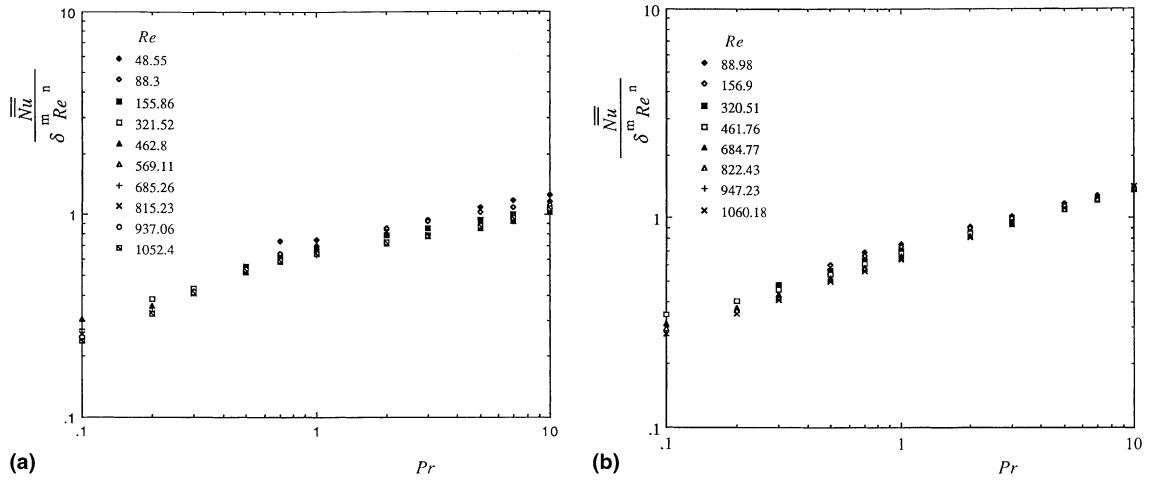

Fig. 10. (a) Nusselt number correlations for CA coil, $Pe > 60$. (b) Nusselt number correlations for AA coil, $Pe > 60$.

power laws. The switching length $z_s = \pi/\delta$, and the switching angle $\theta = 90°$ are kept fixed.

The Nusselt number for the AA coil is of the form

$$\overline{\overline{Nu}} = 0.7\delta^{0.18}Re^{0.5}Pr^{0.375} \quad \text{for } Pr \leqslant 1, \tag{15}$$

$$\overline{\overline{Nu}} = 0.7\delta^{0.18}Re^{0.5}Pr^{0.3} \quad \text{for } Pr > 1, \tag{16}$$

while the CA coil has the dependence

$$\overline{\overline{Nu}} = 0.69\delta^{0.13}Re^{0.5}Pr^{0.43} \quad \text{for } Pr \leqslant 1, \tag{17}$$

$$\overline{\overline{Nu}} = 0.67\delta^{0.13}Re^{0.5}Pr^{0.21} \quad \text{for } Pr > 1. \tag{18}$$

The relative enhancement is thus of the form

$$\frac{\overline{\overline{Nu}}_{AA}}{\overline{\overline{Nu}}_{CA}} = 1.014\delta^{0.05}Pr^{0.055} \quad \text{for } Pr \leqslant 1, \tag{19}$$

$$\frac{\overline{\overline{Nu}}_{AA}}{\overline{\overline{Nu}}_{CA}} = 1.045\delta^{0.05}Pr^{0.09} \quad \text{for } Pr > 1. \tag{20}$$

Fig. 10 shows the Nusselt number correlation data plotted against the Prandtl number for various parameter values with Pr from 0.1 to 10.0, Re from 50 to 1000, and $Pe > 60$. Fig. 10(a) is for the CA coil and Fig. 10(b) is for the AA coil. An assumption implicit in the previous correlations is a boundary layer behavior in-built in the square root scaling of Nu with the Reynolds number. These correlations are valid for $Pe \geqslant 60$.

7. Conclusions

This study establishes quantitatively the viability of using the concept of chaotic mixing as a useful tool in designing an efficient coiled tube heat exchanger. Chaotic mixing is achieved here by periodic rotation of the coil axis which results in an increase in heat transfer in the limit of large Pr. The details of the mechanism responsible for this enhancement are identified. They are associated with the breaking of an interior boundary layer and the degree of convective mixing across this layer. The AA coil geometry displays a heat transfer enhancement of 7–20% in terms of the fully developed Nusselt number with little change in the pressure drop characteristics as compared to a small pitch helical coil idealized as the CA coil over a Reynolds number range of $50 \leqslant Re \leqslant 1200$.

The motivation for studying the periodically developed flow and heat transfer in coiled tubes lies in the possible use of such modules in heat exchangers. Such coiled tube heat exchangers offer the advantages of compactness and increased thermal efficiency. The drawback is geometric complexity which could push up manufacturing and maintenance costs. While the enhancement increases uniformly with the Prandtl number, the coil axis rotation angle, θ, has an optimum value of about 120° at which the enhancement is maximized. For $Pe \geqslant 60$, the enhancement shows little sensitivity to the Reynolds number and the switching length.

Acknowledgements

We are thankful to the Gas Research Institute and the Project Manager, Dr. Ferol Fish for having funded this project under a grant No. 5090-260-1971. We wish to acknowledge the support of the Computing Center at the University of Notre Dame. We also thank Dr. Devadatta Mukutmoni for his help in setting up the numerical model.

References

[1] H. Aref, Stirring by chaotic advection, J. Fluid Mech. 143 (1984) 1–21.

[2] D.V. Khakhar, J.G. Franjione, J.M. Ottino, A case study of chaotic mixing in deterministic flows: the partitioned pipe mixer, Chem. Eng. Sci. (1987) 2909–2926.

[3] S.W. Jones, O.M. Thomas, H. Aref, Chaotic advection by laminar flow in a twisted pipe, J. Fluid Mech. (1989) 335–357.

[4] S. Ghosh, H.-C. Chang, M. Sen, Heat transfer enhancement due to slender recirculation and chaotic transport between counter-rotating eccentric cylinders, J. Fluid Mech. (1992) 119–154.

[5] H. Peerhossaini, Y. Le Guer, Chaotic motion in the Dean instability flow a heat exchanger design, Bull. APS (1990) 2229.

[6] C.S. Lee, J.J. Ou, S.H. Chen, Quantification of mixing from the Eulerian perspective: flow through a curved tube, Chem. Eng. Sci. (1987) 2484–2486.

[7] C. Castelain, A. Mokrani, P. Legentilhomme, H. Peerhossaini, Residence time distribution in twisted pipe flows: helically coiled system and chaotic system, Exp. Fluids 22 (5) (1997) 359–368.

[8] C. Duchene, H. Peerhossaini, P.J. Michard, On the velocity field and tracer patterns in a twisted duct flow, Phys. Fluids 7 (6) (1995) 1307–1317.

[9] S.W. Jones, Chaotic advection and dispersion, Physica 76 (1-3) (1994) 55–69.

[10] S.W. Jones, W.R. Young, Shear dispersion and anomalous diffusion by chaotic advection, J. Fluid Mech. 280 (1994) 149–172.

[11] Y. LeGuer, H. Peerhossaini, Order breaking in Dean flow, Phys. Fluids A (1991) 1029–1032.

[12] A. Mokrani, C. Castelain, H. Peerhossaini, The effects of chaotic advection on heat transfer, Int. J. Heat Mass Transfer 40 (13) (1997) 3089–3104.

[13] H. Peerhossaini, C. Castelain, Y. Leguer, Heat exchanger design based on chaotic advection, Exp. Thermal Fluid Sci. 7 (4) (1993) 333–344.

[14] N. Acharya, M. Sen, H.-C. Chang, Heat transfer enhancement in coiled tubes by chaotic mixing, Int. J. Heat Mass Transfer (1992) 2475–2489.

[15] S.V. Patankar, C.H. Liu, E.M. Sparrow, Fully developed flow and heat transfer in ducts having streamwise-periodic variations of cross-sectional area, ASME J. Heat Transfer (1997) 180–186.

[16] A. Lahbabi, H.-C. Chang, Flow in periodically constricted tubes: transition to inertial and non-steady flows, Chem. Eng. Sci. (1986) 2487–2505.

[17] N. Acharya, Experimental and numerical investigation of heat transfer enhancement in coiled tubes by chaotic mixing, Ph.D. dissertation, University of Notre Dame, Notre Dame, IN, 1992.

[18] J.P. Van Doormaal, G.D. Raithby, Enhancements of the SIMPLE method for predicting incompressible fluid flows, Numer. Heat Transfer (1984) 147–163.

[19] W.R. Dean, Note on the motion of fluid in a curved pipe, Philos. Magazine (1927) 208–223.

[20] A. Wolf, J.B. Swift, H.L. Swinney, Vastano, Determining Lyapunov exponents from time series, Physica D, 16, 1985, pp. 285–317.

[21] N. Acharya, M. Sen, H.-C. Chang, Thermal entrance length and Nusselt numbers in coiled tubes, Int. J. Heat Mass Transfer (1994) 336–340.